MCB
Journals.ASM.org

Mechanism Underlying IκB Kinase Activation Mediated by the Linear Ubiquitin Chain Assembly Complex

Hiroaki Fujita,[a,b,c] Simin Rahighi,[d,e] Mariko Akita,[a] Ryuichi Kato,[d] Yoshiteru Sasaki,[c] Soichi Wakatsuki,[d,e,f] Kazuhiro Iwai[a,c]

Cell Biology and Metabolism Group[a] and Department of Frontier Biosciences,[b] Graduate School of Frontier Biosciences, Osaka University, Suita, Japan; Department of Molecular and Cellular Physiology, Graduate School of Medicine, Kyoto University, Kyoto, Japan[c]; Structural Biology Research Center, Photon Factory, Institute of Materials Structure Science, High-Energy Accelerator Research Organization (KEK), Tsukuba, Ibaraki, Japan[d]; Department of Structural Biology, Stanford University School of Medicine, Stanford, California, USA[e]; SLAC National Accelerator Laboratory, Menlo Park, California, USA[f]

The linear ubiquitin chain assembly complex (LUBAC) ligase, consisting of HOIL-1L, HOIP, and SHARPIN, specifically generates linear polyubiquitin chains. LUBAC-mediated linear polyubiquitination has been implicated in NF-κB activation. NEMO, a component of the IκB kinase (IKK) complex, is a substrate of LUBAC, but the precise molecular mechanism underlying linear chain-mediated NF-κB activation has not been fully elucidated. Here, we demonstrate that linearly polyubiquitinated NEMO activates IKK more potently than unanchored linear chains. In mutational analyses based on the crystal structure of the complex between the HOIP NZF1 and NEMO CC2-LZ domains, which are involved in the HOIP-NEMO interaction, NEMO mutations that impaired linear ubiquitin recognition activity and prevented recognition by LUBAC synergistically suppressed signal-induced NF-κB activation. HOIP NZF1 bound to NEMO and ubiquitin simultaneously, and HOIP NZF1 mutants defective in interaction with either NEMO or ubiquitin could not restore signal-induced NF-κB activation. Furthermore, linear chain-mediated activation of IKK2 involved homotypic interaction of the IKK2 kinase domain. Collectively, these results demonstrate that linear polyubiquitination of NEMO plays crucial roles in IKK activation and that this modification involves the HOIP NZF1 domain and recognition of NEMO-conjugated linear ubiquitin chains by NEMO on another IKK complex.

Nuclear factor κB (NF-κB) is a family of transcription factors that play essential roles in many biological phenomena, including inflammatory responses, cell survival, and innate and acquired immune responses (1). Because aberrant activation of NF-κB signaling is associated with many pathological conditions, such as autoinflammatory diseases and malignancies (2, 3), signal-induced activation of NF-κB has been studied extensively (4). In resting cells, inactive NF-κB resides in the cytoplasm bound to its inhibitor proteins, the inhibitors of κB (IκBs). Stimulation by inflammatory cytokines activates the IκB kinase (IKK) complex, composed of IKK1, IKK2, and NF-κB essential modulator (NEMO). Following phosphorylation by activated IKK, IκBs are degraded by the proteasome, leading to the release of NF-κB, which then translocates to the nucleus to induce transcription of its target genes (5).

The ubiquitin (Ub) conjugation system is deeply involved in the regulation of NF-κB pathway (6). Recent studies showed that the linear ubiquitin chain assembly complex (LUBAC) ligase, which specifically generates linear polyubiquitin chains, is involved in NF-κB activation (7, 8). LUBAC is composed of three subunits: HOIP, HOIL-1L, and SHARPIN. Patients lacking HOIL-1L and mice lacking SHARPIN exhibit immunodeficiency and chronic inflammation, demonstrating the physiological significance of LUBAC-mediated linear polyubiquitination (9–12). In cells from mice lacking HOIL-1L or SHARPIN, the level of the residual LUBAC complex (consisting of the remaining two components) is reduced, and tumor necrosis factor alpha (TNF-α)-induced NF-κB activation is sharply attenuated (9–12). Although NEMO is a target of linear polyubiquitination by LUBAC, it is not yet clear how linear polyubiquitination of NEMO triggers IKK activation.

In this study, using an *in vitro* LUBAC-mediated IKK activation assay, we found that linear diubiquitin conjugation to NEMO potently induces IKK activation. We then dissected the molecular mechanism underlying linear polyubiquitination of NEMO by LUBAC and found that the NPL4 zinc finger 1 (NZF1) domain of HOIP is responsible for recognition of a region in the coiled-coil 2 and leucine zipper (CoZi) domains of NEMO. Mutational analyses based on a cocrystal structure of HOIP NZF1 and NEMO CoZi revealed that HOIP NZF1 binds to NEMO and ubiquitin simultaneously and that both interactions are involved in linear polyubiquitination of NEMO, IKK activation, and subsequent activation of NF-κB. Finally, we showed that homodimerization of IKK2 is involved in linear ubiquitin chain-mediated IKK activation. Taken together, our results suggest that recognition of linear polyubiquitins conjugated to NEMO, possibly by NEMO in another IKK complex, triggers activation of IKK2 by *trans* autophosphorylation.

MATERIALS AND METHODS

RT-PCR and plasmids. The open reading frames (ORFs) of mouse HOIP and NEMO were amplified by reverse transcription-PCR (RT-PCR) of total RNA from C57BL/6 mouse liver. Other cDNAs used in this study were described previously (8, 12). The following full-length proteins, deletion mutants, and fragments were generated from the amplified ORF of HOIP: the wild type (WT) (amino acids 1 to 1066), Δall-ZFs (deletion of amino acids 296 to 432), ΔZF (deletion of amino acids 296 to 325),

Received 20 November 2013 Returned for modification 4 December 2013
Accepted 21 January 2014
Published ahead of print 27 January 2014
Address correspondence to Kazuhiro Iwai, kiwai@mcp.med.kyoto-u.ac.jp, or Simin Rahighi, srahighi@stanford.edu.

doi:10.1128/MCB.01538-13

ΔNZF1 (deletion of amino acids 344 to 373), ΔNZF2 (deletion of amino acids 402 to 432), and NZF1 (amino acids 344 to 382). The following proteins were generated from the amplified ORF of NEMO: the WT (amino acids 1 to 412) and ΔCoZi (deletion of amino acids 250 to 339). Mutations of HOIP (R369A, T354A, F355A, and T354A/F355A), NEMO (Q271A, D275A, Q271A/D275A, K278R, K302R, K278R/K302R, Q271A/D275A/K278R/K302R, F305A, E313A, Q271A/D275A/F305A, and Q271A/D275A/E313A), and IKK2 (V229A/H232A and Y294L/G295K/P296Q) were generated by two-step PCR. cDNAs were ligated to the appropriate epitope tag sequences and then cloned into pcDNA3.1, pcDNA3.1-MMTV (8), pMAL-c2x (New England BioLabs), pGEX-6p1 (GE Healthcare), or MXs-IP (kindly provided by T. Kitamura). pGEX-IκBα (1 to 54) was described previously (8).

Antibodies and reagents. The following antibodies were used: FLAG (M2) (Stratagene); TNFR1 (ab19139) (Abcam); ubiquitin (sc-8017), hemagglutinin (HA; sc-805), glutathione *S*-transferase (GST) (sc-459), maltose binding protein (MBP) (sc-13564), TRADD (sc-7868), and NEMO (sc-8330) (Santa Cruz Biotechnology); FLAG (F7425) (Sigma); T7 (catalog no. 69522) (Novagen); NEMO (K0159-3) (MBL); and pIKK1/2 (catalog no. 2078), RIP1 (catalog no. 3493), pIκBα (catalog no. 9246), and IκBα (catalog no. 4812) (Cell Signaling). His_6-HA-Ub_2, linear di- and tetraubiquitins, and FLAG-His_6–TNF-α (FH-TNF-α) were expressed in *Escherichia coli*. K63 diubiquitin and polyubiquitin chains ($Ub_{1–7}$, Lys63 linked) were purchased from Boston Biochem. Other antibodies and reagents were generated in our laboratory, as described previously (7, 8, 12).

Cell lines, cell cultures, and transfection. NEMO-deficient mouse embryonic fibroblasts (MEFs), N-1 cells (13), HEK293T cells, and HOIP Δlinear MEFs, which were established from mice that express a truncated HOIP (HOIP Δlinear) that lacks the C-terminal catalytic region, were grown in Dulbecco's modified Eagle's medium (DMEM) supplemented with 10% fetal bovine serum (FBS), 100 IU/ml of penicillin, and 100 μg/ml of streptomycin. NEMO-deficient MEFs were kindly provided by H. Kamata (Hiroshima University). NEMO-deficient MEFs stably expressing the NEMO WT or mutants were selected with 150 μg/ml of hygromycin B (Wako) after transfection with WT or mutant pcDNA3.1-MMTV-FLAG-NEMO constructs. N-1 cells stably expressing WT or mutant NEMO, and HOIP Δlinear MEFs stably expressing HOIP WT, ΔNZF1, R369A, or T354A/F355A, were generated using a retroviral expression system, as described previously (12); stable clones were selected with 0.2 μg/ml of puromycin (Sigma-Aldrich) or 500 μg/ml of G418 (Nacalai Tesque). Transfections were performed using Lipofectamine 2000 (Invitrogen).

Immunoprecipitation and immunoblotting. Cells were lysed with lysis buffer containing 50 mM Tris-HCl (pH 7.5), 150 mM NaCl, 1% Triton X-100, 2 mM phenylmethylsulfonyl fluoride (PMSF), and protease inhibitor cocktail (Sigma-Aldrich); lysates were clarified by centrifugation at 15,000 rpm for 20 min at 4°C. For hot lysis, cells were lysed with lysis buffer containing 1% SDS in phosphate-buffered solution (PBS) and then heated at 95°C for 10 min to disrupt noncovalent interactions. After heating, lysates were sheared with a 25-gauge needle and centrifuged at 15,000 rpm for 5 min at room temperature; the resultant supernatant was diluted to 0.1% SDS with lysis buffer containing 50 mM Tris-HCl (pH 7.5), 150 mM NaCl, and 1% Triton X-100. For immunoprecipitations, lysates were incubated with the appropriate antibodies for 2 h on ice and then immobilized on protein A-Sepharose beads (GE Healthcare). The beads were washed five times with buffer containing 50 mM Tris-HCl (pH 7.5), 150 mM NaCl, and 1% Triton X-100. In immunoprecipitations of HA-HOIP, to digest the polyubiquitin chains conjugated to NEMO, the beads were washed two more times with buffer containing 50 mM HEPES-HCl (pH 7.5) and 150 mM NaCl and then incubated with 50 μg/ml of UPS2cc (kindly provided by Rohan Baker [14]) for 1 h at 37°C in buffer containing 50 mM HEPES-HCl (pH 7.5), 150 mM NaCl, and 5 mM dithiothreitol (DTT). Samples were separated by SDS-PAGE and then transferred to polyvinylidene difluoride (PVDF) membranes. After blocking in Tris-buffered saline (TBS) containing 0.1% Tween 20 and 5% (wt/vol) nonfat dry milk, the membranes were incubated with the appropriate primary antibodies, followed by incubation with secondary antibodies. Membranes were visualized using enhanced chemiluminescence and analyzed on an LAS4000mini (Fuji Film).

Protein expression and purification. GST-fused mouse HOIP (amino acids 344 to 382), MBP-fused mouse NEMO (full-length), and mutants derived from either of these fusion proteins were expressed in *E. coli*. Fusion proteins were purified using glutathione-Sepharose (GST-HOIP and derivatives) or amylose resin (MBP-NEMO and derivatives). Recombinant E1, UbcH5c, His_6-HOIP-HOIL-1L-Myc-SHARPIN complex, GST-IκBα (amino acids 1 to 54), linear diubiquitin, and tetraubiquitin were prepared as described previously (7, 8, 15). IKK complex containing HA-IKK1, IKK2, and FLAG-His_6-tagged NEMO (WT or R316A/R319A/E320A mutant) were purified using the baculovirus expression system. IKK complexes were prepared from High Five cells infected with appropriate combinations of baculoviruses, and the complexes were then purified on Ni-nitrilotriacetic acid (Ni-NTA)– agarose. After incubation with Ni-NTA– agarose, bead-bound proteins were treated with 100 U of calf intestinal alkaline phosphatase (New England BioLabs) for 30 min at 37°C, beads were washed with 10 column volumes of 5 mM imidazole, and bound proteins were eluted with 300 mM imidazole.

For crystallization, mouse NEMO CoZi (amino acids 250 to 339) and human HOIP NZF1 (amino acids 350 to 379) proteins were expressed and purified separately and mixed at the proper ratio immediately before crystallization (see next section). To generate expression constructs, NEMO CoZi was cloned into pGEX-4T-1 (GE Healthcare) and HOIPNZF1 was cloned into pGEX-6p-1. The resultant vectors were transformed into *E. coli* BL21, and overexpression of the GST-tagged proteins was induced by addition of 0.5 mM isopropyl-β-D-thiogalactopyranoside (IPTG). After overnight incubation at 25°C, cells were collected and lysed by sonication. The supernatants were applied to glutathione-Sepharose 4B columns (GE Healthcare). The GST tags were cleaved using thrombin/PreScission protease, and proteins were eluted from the columns with PBS buffer. Further purification of the proteins was performed by gel filtration chromatography in a buffer containing 150 mM NaCl and 50 mM Tris-HCl (pH 8.0).

Crystallization, data collection, and structure determination of the NEMO CoZi/HOIP NZF1 complex. Immediately before crystallization, mouse NEMO CoZi and human HOIP NZF1 were mixed in a 2:1 molar ratio (see Fig. 3J for sequence similarity between human and mouse HOIP). Cocrystals were obtained after 6 days of incubation at 20°C in 20% (wt/vol) polyethylene glycol 3350 (PEG 3350) and 0.2 M DL-malic acid (pH 7.0). Single anomalous diffraction (SAD) data were collected to a resolution of 2.0 Å at the Zn atom absorption edge at a wavelength of 1.28 Å. The data were collected at 100 K at the beamline NW-12A of the KEK Photon Factory (Tsukuba, Japan) using HKL2000 (16) and processed by iMosflm (17). Because SAD using the anomalous signal from the single zinc atom did allow successful phasing, the structure was solved by the molecular replacement (MR) method using MOLREP (18) from the CCP4 package (Collaborative Computational Project, number 4, 1994). The structures of NEMO CoZi (PDB entry 3FX0) (19) and TAB2 NZF (PDB entry 2WX0) (20) were used as search models for MR. One complex containing two NEMO molecules (as a dimer) and one HOIP NZF1 molecule was found in each asymmetric unit of the crystal, which belonged to the $P6_5$ space group. The anomalous signal from Zn atoms was used to confirm the position of the Zn atom in the complex structure solved by MR. The model was further built and refined using COOT (21) and REFMAC5 (22, 23). After the final refinement, NEMO CoZi amino acids 252 to 336 and 251 to 337 (from the two protomers) and HOIP NZF1 amino acids 351 to 379 were clearly visible in the electron density map. Data collection and refinement statistics are summarized in Table 1. All structure figures were prepared using PyMOL (DeLano Scientific; http://www.pymol.org).

***In vitro* IKK activation assay.** Twenty-microliter samples containing the following were incubated for 1 h at 30°C: 50 mM Tris-HCl (pH 7.5), 5

TABLE 1 Data collection and refinement statistics

Parameter	Value(s) for NEMO CoZi/HOIP NZF1 complex
Data collection statistics	
Space group	$P6_5$
Cell dimensions	
a, *b*, *c* (Å)	81.46, 81.46, 74.57
α, β, γ (°)	90.00, 90.00, 120.00
Wavelength (Å)	1.282
Resolution (Å)	33.0–2.00 (2.05–2.00)[a]
R_{merge}	0.14 (1.11)
$I/\sigma I$	7.7 (1.1)
Completeness (%)	83.1 (66.6)
Redundancy	7.6 (6.8)
CC1/2[c]	0.99 (0.63)
Refinement statistics	
Resolution (Å)	50.00–2.00
No. of reflections	17,945
R_{work}/R_{free}[b]	25.9/31.3
No. of:	
Atoms	1,743
Proteins	1,642
Water	100
Ion	1
B factors (Å^2)	
Protein	34.4
Water	36.6
Ions	20.6
RMS deviation	
Bond lengths (Å)	0.011
Bond angles (°)	1.369
Ramachandran statistics	
Residues in most favored regions (%)	97.3
Residues in additionally allowed regions (%)	2.7
Residues in generously allowed regions (%)	0.0
Residues in disallowed regions (%)	0.0

[a] The values in parenthesis relate to the highest-resolution shells.
[b] R_{free} was calculated for a randomly chosen 5% of reflections; the *R* factor was calculated for the remaining 95% of reflections.
[c] CC1/2, a correlation coefficient calculated between one half of the intensity observations (chosen at random) and the other half.

mM $MgCl_2$, 1 mM DTT, 2 mM ATP, 10 mM creatine phosphate, 50 μg/ml of creatine phosphokinase, phosphatase inhibitor cocktail (Nacalai Tesque), 5 μg/ml of E1, 20 μg/ml of UbcH5c, 10 μg/ml of LUBAC, and 5 μg/ml of GST-IκBα (1 to 54); 250 μg/ml of ubiquitin or 10, 50, or 250 μg/ml of His_6-HA-Ub_2 (Fig. 1C); and 0.5, 2.5, or 5 μg/ml (Fig. 1A) or 1 μg/ml (Fig. 1B and C) of IKK complex.

For Fig. 1B, the first ubiquitination reaction was performed in a reaction mixture containing 50 mM Tris-HCl (pH 7.5), 5 mM $MgCl_2$, 1 mM DTT, 10 mM creatine phosphate, 50 μg/ml of creatine phosphokinase, 5 μg/ml of E1, 20 μg/ml of UbcH5c, 10 μg/ml of LUBAC, and 375 μg/ml of ubiquitin in the presence or absence of 2 mM ATP. The reaction ran for 90 min at 30°C; the first reaction was stopped by addition of EDTA (10 mM) and DTT (5 mM), and the reaction mixture was incubated for 15 min at room temperature to release ubiquitin from E1, E2, and LUBAC. *N*-Ethylmaleimide (NEM; 20 mM final concentration) was then added, and the reaction mixture was incubated for 15 min at room temperature to inactivate E1, E2, and LUBAC, after which DTT (10 mM final concentration) was added to inactivate excess NEM. Samples were then dialyzed against buffer containing 50 mM Tris-HCl (pH 7.5) and 5 mM $MgCl_2$ to remove NEM, DTT, and EDTA. In the second-step reaction, the dialyzed mixture containing 0.2, 1, or 5 μg of ubiquitin or linear ubiquitin chains was incubated with 1 μg/ml of IKK complex and 5 μg/ml of GST-IκBα (amino acids 1 to 54) in a reaction mixture containing 50 mM Tris-HCl (pH 7.5), 5 mM $MgCl_2$, 1 mM DTT, 2 mM ATP, 10 mM creatine phosphate, and 50 μg/ml of creatine phosphokinase in the presence or absence of 5 μg/ml of E1, 20 μg/ml of UbcH5c, and 10 μg/ml of LUBAC.

GST and MBP pulldown assays. Five-microgram quantities of GST-fused WT and mutant HOIP NZF1 proteins were immobilized on glutathione-Sepharose FF beads and then incubated for 1 h at 4°C with 1 μg of K63 diubiquitin or linear tetraubiquitin in buffer containing 20 mM Tris-HCl (pH 7.5), 40 μM zinc chloride, 1 mM DTT, 150 mM NaCl, and 0.1% Triton X-100. The beads were washed three times with the same buffer.

Ten-microgram quantities of MBP-fused WT and mutant NEMO proteins were immobilized on amylose resin and then incubated with 1 μg of K63-diubiquitin in the presence or absence of 1 μg of GST-NZF1, 5 μg of linear tetraubiquitin, or 1 μg of K63-$Ub_{1–7}$ for 1 h at 4°C in buffer containing 20 mM Tris-HCl (pH 7.5), 1 mM DTT, 150 mM NaCl, and 0.1% Triton X-100. The beads were washed three times with the same buffer, boiled in SDS sample buffer, and analyzed by immunoblotting.

***In vitro* ubiquitination assay.** Twenty-microliter samples containing 50 mM Tris-HCl (pH 7.5), 5 mM $MgCl_2$, 1 mM DTT, 2 mM ATP, 10 mM creatine phosphate, 50 μg/ml of creatine phosphokinase, 5 μg/ml of E1, 20 μg/ml of UbcH5c, 0.5 μg/ml of LUBAC, 1 μg/ml of WT MBP-NEMO or Q271A/D275A mutant, and 50 μg/ml of ubiquitin were incubated at 37°C for 1 h. The reaction mixtures were subjected to immunoblotting with anti-MBP antibody.

Luciferase assays. HEK293T cells were transfected with pGL4.32 (Luc2p/NF-κB-RE/Hygro) and pGL4.74 (hRLuc/TK) (Promega), along with expression plasmids for WT or mutant HA-HOIP, Myc-HOIL-1L, and T7-SHARPIN. Twenty-four hours after transfection, cells were lysed, and luciferase activities were measured on a Lumat luminometer (Berthold) using the dual-luciferase reporter assay system (Promega). N-1 cells were transfected with reporter plasmids, as described above, along with pcDNA3.1-MMTV expression plasmid for WT or mutant NEMO. Sixteen hours after transfection, cells were stimulated with interleukin 1β (IL-1β; 1 ng/ml) for 8 h, and luciferase activities were measured as described above.

***In vitro* IKK kinase assay.** NEMO-deficient MEFs stably expressing WT or Q271A/D275A NEMO were treated with TNF-α (10 ng/ml) and lysed. IKK complexes were immunoprecipitated with anti-NEMO antibody. The anti-NEMO immunoprecipitates were incubated with GST-IκBα (amino acids 1 to 54) for 2 h at 30°C in kinase buffer (50 mM Tris-HCl [pH 7.5], 5 mM $MgCl_2$, 2 mM ATP, 10 mM creatine phosphate, 50 μg/ml of creatine kinase, and phosphatase inhibitor cocktail). The reaction mixtures were subjected to immunoblotting with anti-pIκBα, anti-NEMO, and anti-GST.

TNFR1 immunoprecipitation. HOIP Δlinear MEFs retrovirally expressing WT HOIP or the ΔNZF1, R369A, or T354A/F355A mutant were treated with FH-TNF-α (3 μg/ml); cells were lysed with lysis buffer containing 10 mM Tris-HCl (pH 7.5), 150 mM NaCl, 0.2% NP-40, 10% glycerol, 2 mM PMSF, and protease inhibitor cocktail (Sigma-Aldrich), followed by centrifugation at 10,000 × *g* for 20 min at 4°C. The TNFR1 complex was immunoprecipitated by incubation with 30 μl of M2 antibody-coupled Dynabeads protein G (Novex by Life Technologies) at 4°C for 90 min. The precipitates were washed five times with the same lysis buffer. The immunoprecipitated TNFR1 complex was eluted by incubation at 37°C for 40 min in 30 μl of TBS buffer containing 400 ng/μl of 3× FLAG peptide (Sigma) and then analyzed by Western blotting.

Protein structure accession number. Atomic coordinates and structure factors of the NEMO CoZi/HOIP NZF1 complex structure have been deposited in the Protein Data Bank under accession number 4O4M.

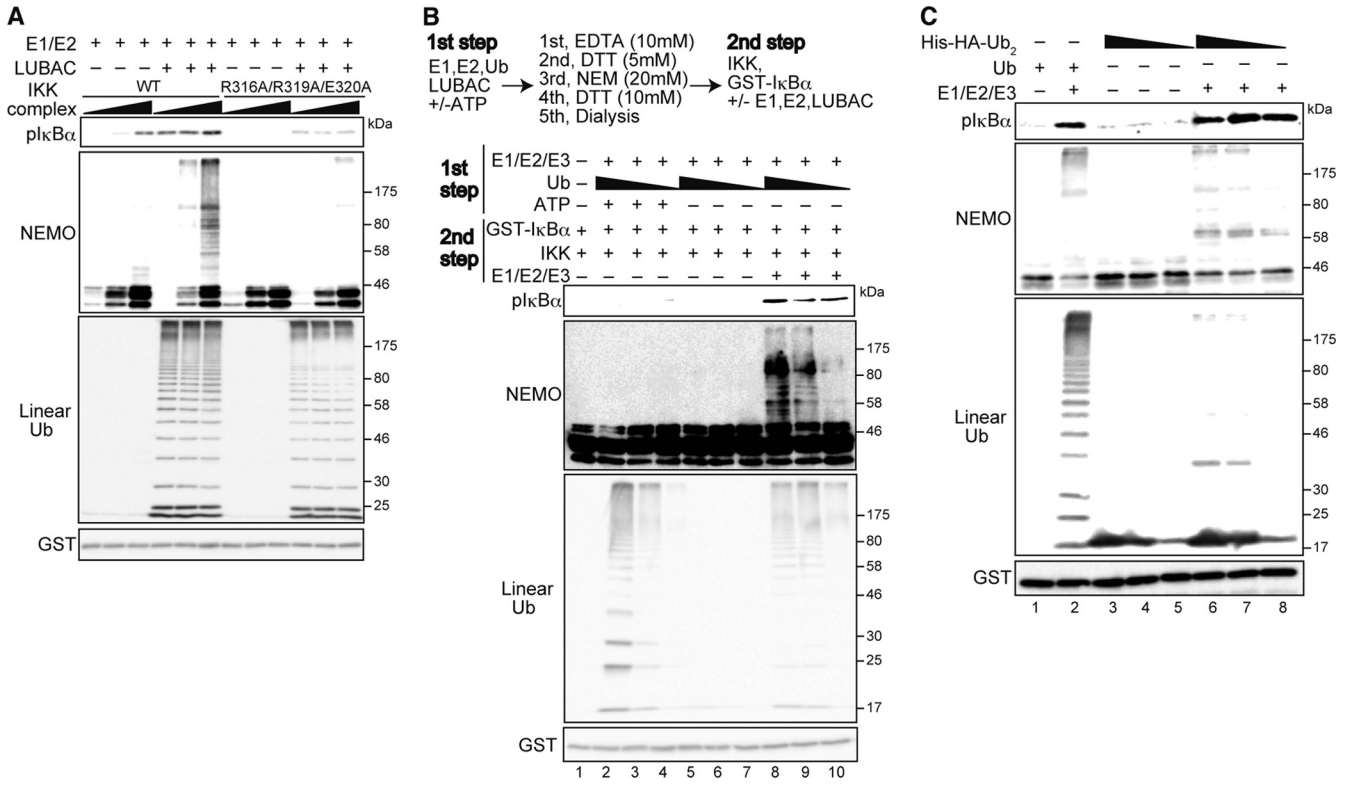

FIG 1 Linearly ubiquitinated NEMO activates the IKK complex more efficiently than unanchored linear ubiquitin chains. (A) IKK complex (0.5, 2.5, or 5 μg/ml) containing either WT or R316A/R319A/E320A NEMO was incubated for 1 h at 30°C with GST-IκBα (amino acids 1 to 54), E1, and UbcH5c in the presence or absence of LUBAC, and the reaction mixtures were probed with the indicated antibodies. (B) Reaction mixtures containing E1, E2, LUBAC, and ubiquitin were incubated with or without ATP. After incubation, E1, E2, and LUBAC were inactivated with EDTA and NEM, and the reaction mixtures were dialyzed. The dialyzed samples were incubated with GST-IκBα (amino acids 1 to 54) and the IKK complex in the presence or absence of E1, E2, and LUBAC, followed by probing with the indicated antibodies. (C) His-HA-Ub_2 (10, 50, or 250 μg/ml) or 250 μg/ml of ubiquitin was incubated with E1, UbcH5c, LUBAC, IKK complex, and GST-IκBα (amino acids 1 to 54), followed by probing with the indicated antibodies.

RESULTS

IKK is effectively activated by linear polyubiquitin conjugated to NEMO but not by unanchored linear polyubiquitin. To investigate in detail the roles of linear polyubiquitination of NEMO in IKK activation, we established an *in vitro* IKK activation assay using purified proteins. In this assay, baculovirus-purified IKK complex containing NEMO WT, or a NEMO mutant in which the critical residues for ubiquitin-binding activity were mutated to Ala (R316A/R319A/E320A in human NEMO, equivalent to R309A/R312A/E313A in mouse NEMO) (24), was incubated with GST-IκBα (amino acids 1 to 54), E1, E2, and ubiquitin in the presence or absence of LUBAC (Fig. 1A). When incubated with the IKK complex containing NEMO WT, LUBAC generated unanchored linear chains, conjugated these linear chains to NEMO, and promoted the phosphorylation of IκBα. Phosphorylation of IκBα was also induced when a high concentration of IKK containing NEMO WT was incubated without LUBAC, possibly due to partial activation of the IKK complex during purification. However, in the presence of IKK complex containing R316A/R319A/E320A NEMO, no detectable IKK activity was induced, although generation of unconjugated linear chains was not affected by the mutation. Although the NEMO mutant was linearly ubiquitinated much more weakly than WT NEMO, we could detect linear ubiquitination when a high concentration of the NEMO mutant was incubated. These results indicated that the ubiquitin-binding activity of NEMO is involved in IKK activation, but it remains unclear why the linear ubiquitination of NEMO was suppressed by the R316A/R319A/E320A mutation.

Both unanchored linear ubiquitin chains and linearly ubiquitinated NEMO were generated when IKK complex containing WT NEMO was activated (Fig. 1A). Therefore, to determine whether unanchored linear ubiquitin chains and/or linearly ubiquitinated NEMO is involved in IKK activation, we incubated E1, E2, LUBAC, and ubiquitin in the presence or absence of ATP, followed by treatment with DTT, EDTA, and NEM to inactivate E1, E2, and LUBAC and disassemble E1- and UbcH5c-ubiquitin (Fig. 1B). After incubation with DTT to inactivate excess NEM and dialysis to remove NEM, DTT, and EDTA, the mixture was incubated with the IKK complex and GST-IκBα (amino acids 1 to 54) in the presence or absence of E1, E2, and LUBAC. IκBα phosphorylation was not induced when neither unanchored nor NEMO-conjugated linear chains were generated (Fig. 1B, lanes 5 to 7), but efficient IκBα phosphorylation was observed in samples in which both unconjugated and NEMO-conjugated linear chains were generated in the second-step reaction (Fig. 1B, lanes 8 to 10). However, IκBα was not efficiently phosphorylated in samples in which unanchored linear chains, but not NEMO-conjugated linear chains, were generated in the first-step reaction (Fig. 1B, lanes 2 to 4). The unanchored linear chains generated in the first-step reaction appeared to be intact because they could bind the ubiquitin-binding domain of NEMO

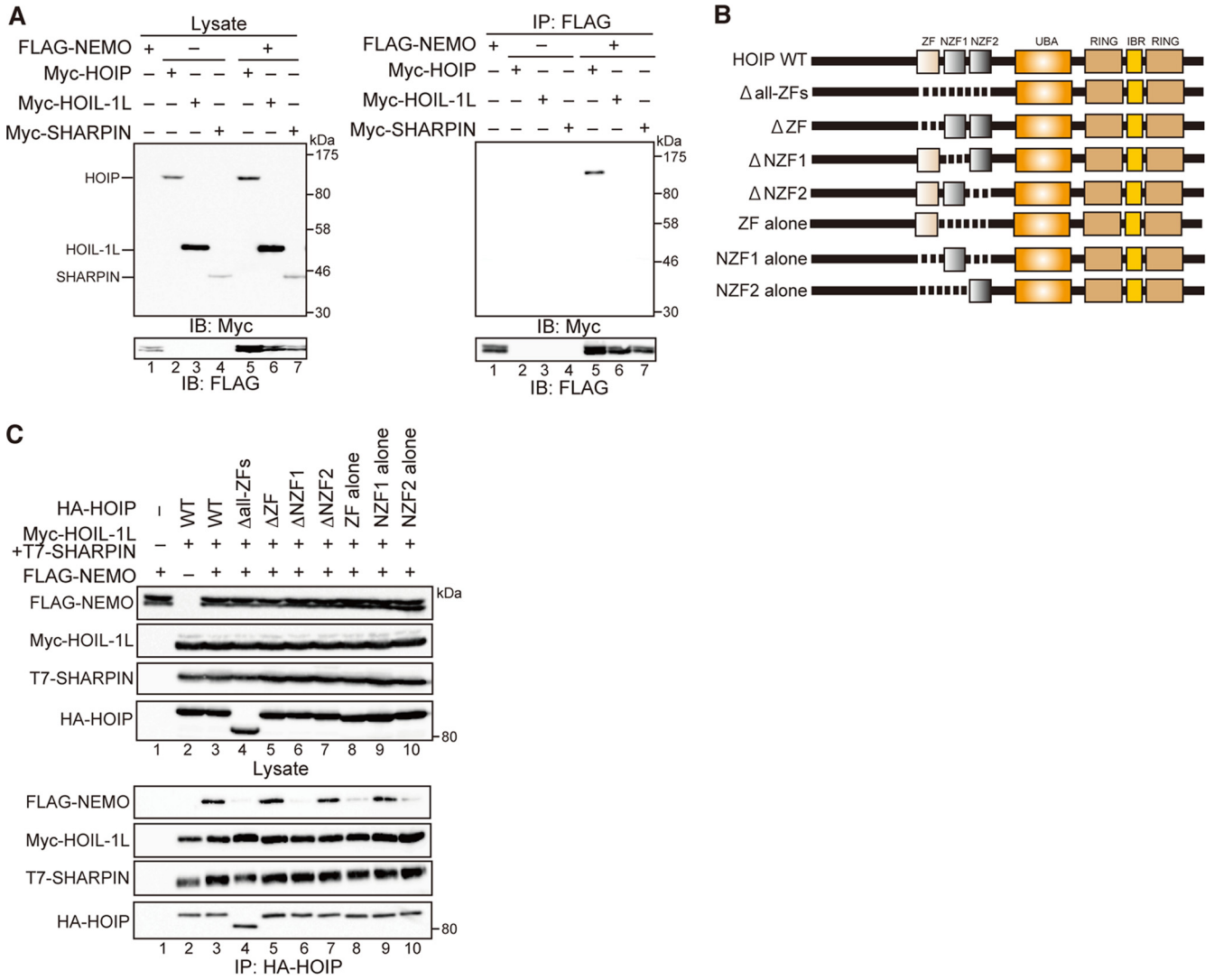

FIG 2 The NZF1 domain of HOIP is responsible for NEMO binding. (A) Myc-HOIP, Myc-HOIL-1L, or Myc-SHARPIN was transfected into HEK293T cells with or without FLAG-NEMO, and cell lysates and anti-FLAG immunoprecipitates (IP) were immunoblotted with the indicated antibodies. (B) Schematics of HOIP and its mutants. (C) HA-HOIP and its mutants, along with Myc-HOIL-1L, T7-SHARPIN, and FLAG-NEMO, were transfected into HEK293T cells. Cell lysates (top) and anti-HA immunoprecipitates (bottom) were immunoblotted with the indicated antibodies.

(data not shown); moreover, ubiquitin contains no Cys residues and therefore cannot be modified by NEM. In our previous analyses, unanchored linear diubiquitin weakly activated IKK *in vitro* (15). To confirm that linear chains conjugated to NEMO activate the IKK complex much more efficiently than unanchored linear polyubiquitin, and to determine the length of linear chains that is sufficient to activate IKK, we incubated N-terminally His_6-HA-tagged diubiquitin (His-HA-Ub_2), instead of ubiquitin monomers, in the presence or absence of E1, E2, and LUBAC (Fig. 1C). His-HA-Ub_2 can be recognized by the ubiquitin-binding domain of NEMO and then conjugated to substrates, but it cannot generate linear chains longer than diubiquitin because of its N-terminal His_6-HA tag (25). Free His-HA-Ub_2 did not overtly activate IKK (Fig. 1C, lanes 3 to 5), indicating that unanchored diubiquitin cannot activate IKK effectively. However, IKK was effectively activated when His-HA-Ub_2 was conjugated to NEMO by LUBAC (Fig. 1C, lanes 6 to 8). This result confirmed that linear chains conjugated to NEMO activate the IKK complex much more effectively than unanchored linear chains and that conjugation of linear diubiquitin to NEMO is sufficient to activate IKK.

The HOIP NZF1 domain is involved in the recognition of NEMO by LUBAC. Because ubiquitination often requires substrate binding by E3 enzymes (26), we hypothesized that LUBAC may also recognize NEMO prior to linear polyubiquitination of the protein. To dissect the molecular mechanism underlying linear polyubiquitination of NEMO, we probed the region of the LUBAC ligase complex that is critical for recognition of NEMO. To this end, we first expressed each subunit of LUBAC (HOIL-1L, HOIP, and SHARPIN) in HEK293T cells, with or without NEMO. Consistent with our observations in a previous study (8), HOIP coimmunoprecipitated with NEMO (Fig. 2A, lane 5). In the earlier study, deletion of the zinc finger region, containing the zinc finger (ZF), NZF1, and NZF2 domains, attenuated the interaction between HOIP and NEMO, although HOIP Δall-ZFs could still

bind to NEMO when the two proteins were coexpressed with HOIL-1L. In contrast, in this study, HOIP Δall-ZFs did not efficiently interact with NEMO even in the presence of HOIL-1L and SHARPIN (Fig. 2B and C, lane 4). The discrepancy between these observations might be attributed to the amounts of plasmids used in the transfections: in the previous study, we introduced larger amounts of the plasmids into cells than in this study.

To precisely determine the roles played by the three domains of the HOIP ZF region in the interaction with NEMO, we cotransfected WT or mutant HOIP (Fig. 2B) into HEK293T cells along with HOIL-1L, SHARPIN, and NEMO and assessed the binding between NEMO and HOIP (Fig. 2C). Among the three domains in the zinc finger region, deletion of HOIP NZF1, but not deletion of ZF or NZF2, attenuated NEMO binding (Fig. 2C, lanes 5 to 7). Conversely, among HOIP mutants possessing only one of the three zinc finger domains, mutants containing NZF1 but not ZF or NZF2 could bind NEMO (Fig. 2C, lanes 8 to 10). These results strongly indicated that HOIP NZF1 is sufficient for the recognition of NEMO. To characterize the region of NEMO that is recognized by HOIP, we introduced NEMO mutants into HEK293T cells together with HOIL-1L, HOIP, and SHARPIN (data not shown); these experiments confirmed our previous observation (8) that NEMO lacking the CoZi region failed to bind LUBAC.

Crystal structure of NEMO CoZi in complex with HOIP NZF1. To obtain further insight into the recognition of NEMO by HOIP, we determined the crystal structure of the complex between the NEMO CoZi and HOIP NZF1 domains (Table 1). The crystal structure contains one complex per asymmetric unit, in which NEMO and HOIP are present in 2:1 stoichiometry, i.e., each NEMO dimer binds one NZF1 molecule (Fig. 3A). Despite the symmetrical surface on either side of NEMO, each NEMO dimer binds only one HOIP NZF1. This appears to be due to crystal packing effects, because another HOIP NZF1 of a symmetry-related molecule occupies the second possible binding site on NEMO. This binding mode includes weak interactions between NEMO and another surface of HOIP centered on residues Thr360 and Phe361, which, according to our mutational analyses, are not biologically relevant (see below and Fig. 7C). However, this observation does not exclude the possibility of symmetrical binding of two HOIP NZF1 molecules to NEMO in solution or *in vivo*, which might be influenced by factors such as the local concentration of proteins (27). In the context of the full-length proteins, however, it seems more likely that binding of a large LUBAC would hinder binding of a second HOIP NZF1 domain to a NEMO molecule. In fact, due to the transient nature of these interactions, to date we have been unable to measure the stoichiometry of NEMO CoZi/HOIP NZF-1 binding using the isolated domains in solution.

In the crystal structure, HOIP NZF1 forms a compact structure typical of NZF domains (Fig. 3A) (28), with a single zinc ion coordinated by four conserved cysteine residues: Cys356, Cys359, Cys370, and Cys373. As shown previously, NEMO CoZi forms a coiled-coil homodimeric structure (19, 24). Although NEMO CoZi bound to HOIP NZF1 retains a conformation similar to that of the free domain, the overall structures do not superimpose well, as indicated by the root mean square (RMS) deviation of 2.6 Å for superimposition of the Cα atoms of residues 255 to 335 (Fig. 3B). This structural difference appears to be due to the presence of a proline residue (Pro292) in the CoZi domain, which introduces a kink into the coiled-coil structure (24). Consistent with this explanation, the two regions N terminal and C terminal to Pro292 (amino acids 255 to 291 and 293 to 335, respectively) superimpose more precisely (RMS deviations of 1.1 Å and 1.3 Å, respectively) (Fig. 3C and D).

The HOIP NZF1 binding site on NEMO is located on the coiled-coil 2 (CC2) domain and covers a surface area of 447.3 $Å^2$. The binding region includes amino acid residues from Gln259 to Lys270 and Glu264 to Asp275 on different protomers within the NEMO dimer (Fig. 3E and F). This surface is located at the N terminus of NEMO CoZi and does not overlap the ubiquitin-binding domain (UBAN) (24). Thus, interaction with HOIP does not sterically hinder binding of NEMO to linear ubiquitin chains (Fig. 3A).

A hydrophobic surface on the NZF1 domain, formed by the side chains of Ala366, Val368, Leu369, Pro376, Leu378, and Ala379, serves as the major interacting partner for NEMO by contacting Ala263, Ala266, Leu267, Val268, and aliphatic portions of Gln259, Lys270, and Gln271 (Fig. 3G and H). Furthermore, Glu374, Arg375, and Arg377 from HOIP are engaged in electrostatic interactions with Lys270, Asp275, and Glu264, respectively. The Nε atom of NEMO Gln259 forms a hydrogen bond with the main-chain carbonyl oxygen of Ala365 (Fig. 3G). Although it is not conserved among other NZF domains, the NEMO-binding surface on HOIP NZF1 is highly conserved among HOIP proteins from different species (Fig. 3I and J).

Gln271 and Asp275 of NEMO are involved in LUBAC-mediated linear polyubiquitination. Our structural analysis indicated that Gln271 and Asp275 of mouse NEMO are involved in the interaction with the HOIP NZF1 domain (Fig. 3). To confirm the importance of NEMO recognition by HOIP in linear polyubiquitination of NEMO, we generated the NEMO mutations Q271A, D275A, and Q271A/D275A and introduced them into HEK293T cells together with HOIP, HOIL-1L, and SHARPIN. Whereas WT NEMO efficiently coimmunoprecipitated with HOIP, the interactions between HOIP and the Q271A, D275A, and Q271A/D275A NEMO mutants were significantly attenuated (Fig. 4A), suggesting that Gln271 and Asp275 of NEMO are involved in recognition by HOIP *in vivo*. We also confirmed that Q271A/D275A NEMO could efficiently form the canonical IKK complex with IKK1 and IKK2 (Fig. 4B). The ubiquitin-binding activity of NEMO plays essential roles in NF-κB activation (24). Therefore, we compared the abilities of WT, Q271A, D275A, and Q271A/D275A NEMO to bind linear and Lys63-linked polyubiquitins. All three of the NEMO mutants interacted with both linear tetraubiquitin and Lys63-linked ubiquitin chains as efficiently as WT NEMO, which can bind both linear and Lys63 chains (longer than four ubiquitin moieties) (Fig. 4C and D) (29). These results confirmed the finding that Gln271 and Asp275 are not located in the ubiquitin-binding domain of NEMO (Fig. 3A).

We next assessed the effect of Gln271 and/or Asp275 mutation of NEMO on its linear polyubiquitination in an *in vitro* ubiquitination assay and found that Q271A/D275A NEMO was not efficiently ubiquitinated by LUBAC (Fig. 4E). To confirm the attenuation of linear polyubiquitination of NEMO mutants that failed to interact efficiently with HOIP in cells, we introduced WT or mutant NEMO along with the components of LUBAC into HEK293T cells and then performed hot lysis to remove proteins noncovalently associated with NEMO (Fig. 4F). Although WT NEMO was efficiently linearly polyubiquitinated by LUBAC, linear polyubiquitination of Q271A, D275A, and Q271A/D275A NEMO was significantly attenuated.

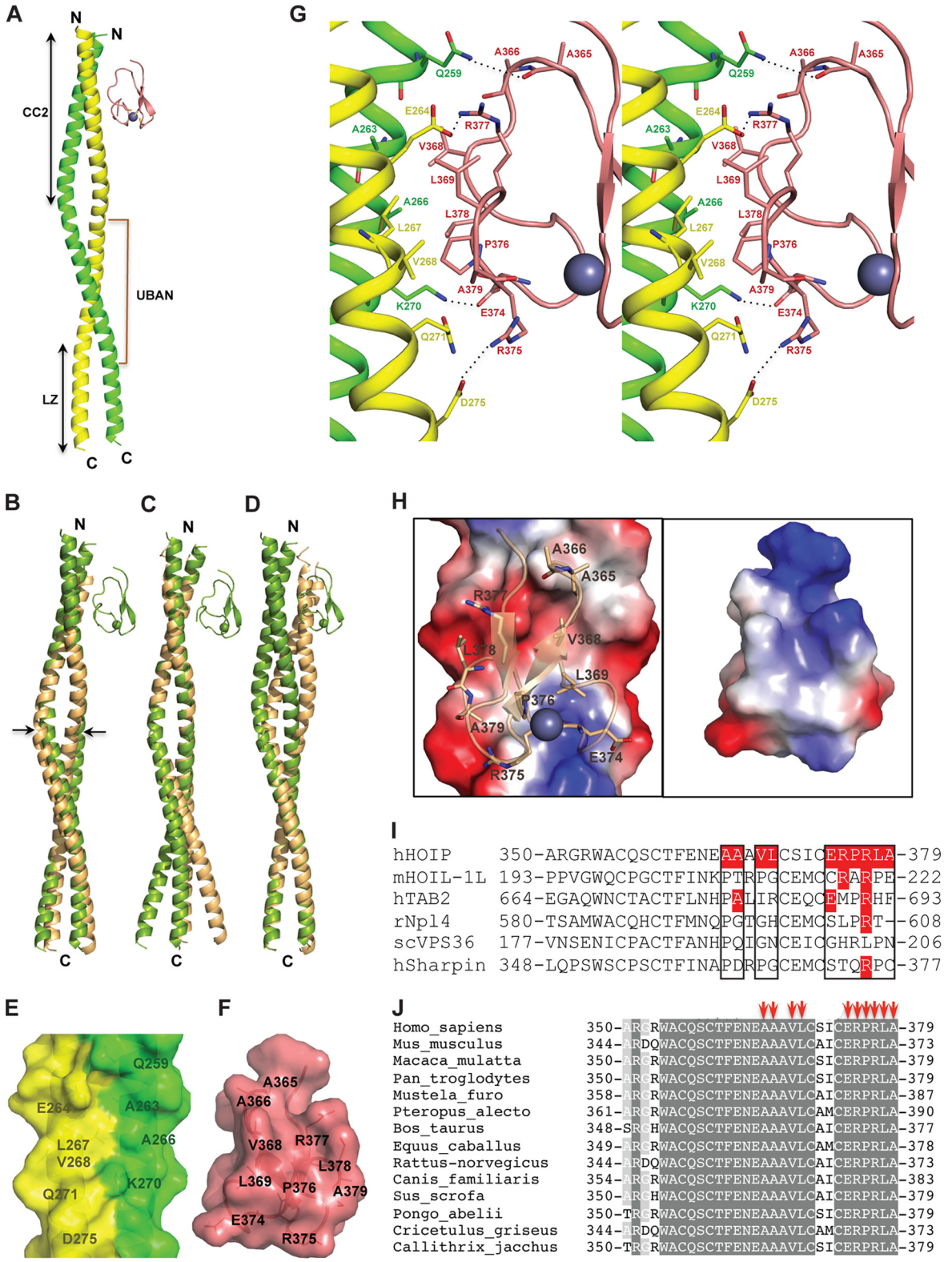

FIG 3 Structure of the NEMO CoZi in complex with HOIP NZF1. (A) Overall structure of the NEMO CoZi/HOIP NZF1 complex. The two chains of NEMO are colored in yellow and green; HOIP is shown in salmon. The CC2 and CoZi (LZ) and UBAN (ubiquitin-binding in ABIN proteins and NEMO) domains are indicated on the NEMO structure. (B to D) Superimposition of the NEMO molecules in the free form (light orange) and in complex with HOIP NZF1 (green), including residues 255 to 335 (B), 255 to 291 (C), and 293 to 335 (D). Arrows indicate position of the Pro292 residues in the NEMO structure. (E and F) Amino acid residues involved in the interactions are indicated on the surfaces of NEMO (E) and HOIP (F). (G) Stereo view of the interactions between NEMO CoZi and HOIP NZF1. Interacting amino acids are shown as sticks. Salt bridges and hydrogen bonds are indicated with dashed lines. (H) Open-book representation of NEMO recognition by HOIP NZF1. (I) Analysis of conservation of residues of HOIP NZF1 involved in binding to NEMO in different NZF domain-containing proteins. Interacting residues from HOIP NZF1 and conserved residues are highlighted in red. (J) Analysis of conservation of residues of HOIP NZF1 involved in binding to NEMO in various species. Highly conserved residues are highlighted in dark gray, and less conserved residues are in light gray. The arrows indicate residues from human HOIP that interact with NEMO.

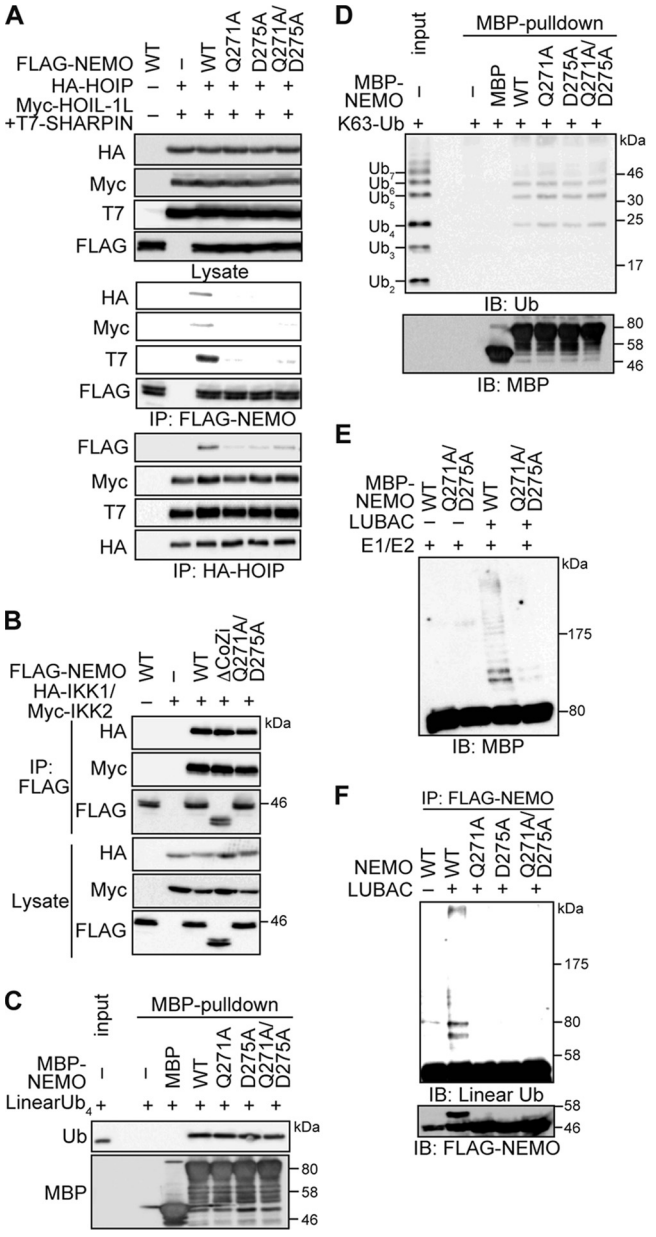

FIG 4 Involvement of Gln271 and Asp275 of NEMO in LUBAC-mediated linear polyubiquitination. (A) HEK293T cells were transfected as indicated, and cell lysates (top), anti-FLAG immunoprecipitates (middle), and anti-HA immunoprecipitates (bottom) were immunoblotted. (B) HEK293T cells were transfected as indicated, and cell lysates (bottom) and anti-FLAG immunoprecipitates (top) were immunoblotted. (C and D) NEMO WT or mutants fused with MBP were incubated with linear tetraubiquitin (C) or K63 chains (D), followed by pulldown with maltose resins. (E) WT or Q271A/D275A MBP-NEMO was incubated as indicated at 37°C for 1 h, followed by immunoblotting with anti-MBP antibody. (F) FLAG-NEMO or its mutants were introduced into HEK293T cells together with LUBAC. Cells were subjected to hot lysis, and anti-FLAG immunoprecipitates were probed with anti-linear ubiquitin or anti-FLAG antibody.

Involvement of both linear chain conjugation to NEMO and linear chain recognition by NEMO in IKK activation. Because the NEMO mutants (Q271A, D275A, and Q271A/D275A mutants) could not be recognized or linearly polyubiquitinated by LUBAC but could form IKK complexes with IKK1 and IKK2 and bind to ubiquitin chains as well as WT NEMO, they appeared to be suitable tools for probing the roles of linear polyubiquitination of NEMO in signal-induced NF-κB activation. We therefore transiently introduced WT or mutant NEMO, together with the 5× NF-κB luciferase reporter, into a NEMO-deficient subclone (N-1) of the Rat-1 fibroblast line. Luciferase assays revealed that the Q271A, D275A, and Q271A/D275A mutations of NEMO attenuated IL-β-induced NF-κB activation (Fig. 5A, upper portion). The introduced WT and mutant NEMO proteins were expressed at almost identical levels (Fig. 5A, lower portion) that were slightly lower than the level of endogenous NEMO expression in the parental Rat-1 cells (data not shown). When WT or Q271A/D275A NEMO was retrovirally introduced into the NEMO-defective N-1 cells, IL-1β-induced linear polyubiquitination and IκBα phosphorylation were significantly attenuated by the Q271A/D275A mutation (Fig. 5B). We also stably introduced WT or Q271A/D275A NEMO into the NEMO-deficient MEFs; these proteins were expressed at levels comparable to, or slightly lower than, that of endogenous NEMO in WT MEFs (data not shown). In the NEMO-deficient MEFs complemented with WT NEMO, treatment with TNF-α induced phosphorylation and degradation of IκBα (Fig. 5C). In contrast, in cells expressing Q271A/D275A NEMO, TNF-α-mediated phosphorylation and degradation of IκBα were significantly attenuated (Fig. 5C). Furthermore, TNF-α induced the IKK activity in anti-NEMO immunoprecipitates from cells expressing WT NEMO, whereas TNF-α did not overtly induce IKK activity in Q271A/D275A NEMO-expressing cells (Fig. 5D).

Lys278 and Lys302 of mouse NEMO, which are equivalent to Lys285 and Lys309 of human NEMO, are major sites of linear polyubiquitination by LUBAC (8). The UBAN motif, the major ubiquitin-binding site of NEMO, preferentially binds to linear diubiquitin relative to Lys63-linked diubiquitin. Within this motif, Phe305 is involved in the binding of both linear and Lys63-linked diubiquitin, whereas Glu313 is specifically involved in linear diubiquitin recognition (24). To investigate the functional interaction between HOIP binding and linear polyubiquitination of, or recognition of linear ubiquitin chains by, NEMO, we transiently expressed the NEMO mutants indicated in Fig. 6A in N-1 cells and assessed IL-1β-induced NF-κB activation by luciferase assays. The introduced WT and mutant forms of NEMO were expressed at almost identical levels (Fig. 6A) that were slightly lower than the endogenous NEMO expression level in the parental Rat-1 cells (data not shown). Introduction of mutations at the major polyubiquitination sites, K278R/K302R (QDKK/AARR), into Q271A/D275A NEMO failed to further suppress IL-1β-induced NF-κB activation attenuated by Q271A/D275A mutation, thus confirming that the NEMO recognition by NZF1 of HOIP attenuates LUBAC-induced linear polyubiquitination of the protein. Mutation of Glu313 to Ala (NEMO E313A) marginally suppresses NF-κB activation by partially impairing linear chain binding (24), an observation confirmed in this study (Fig. 6A). To investigate whether impaired recognition of linear ubiquitin chains and NEMO would additively suppress IL-1β-induced NF-κB activation, we generated Q271A/D275A/E313A (QD/AA/E313A) NEMO. This triple mutant attenuated IL-1β-induced NF-κB activation to a greater extent than Q271A/D275A or E313A NEMO. However, the F305A NEMO mutation, which abolishes NEMO binding to both linear and Lys63-linked chains almost completely (24), strongly suppressed IL-1β-induced NF-κB activation, confirming the importance of ubiquitin binding by NEMO for NF-κB activation. These results suggested that

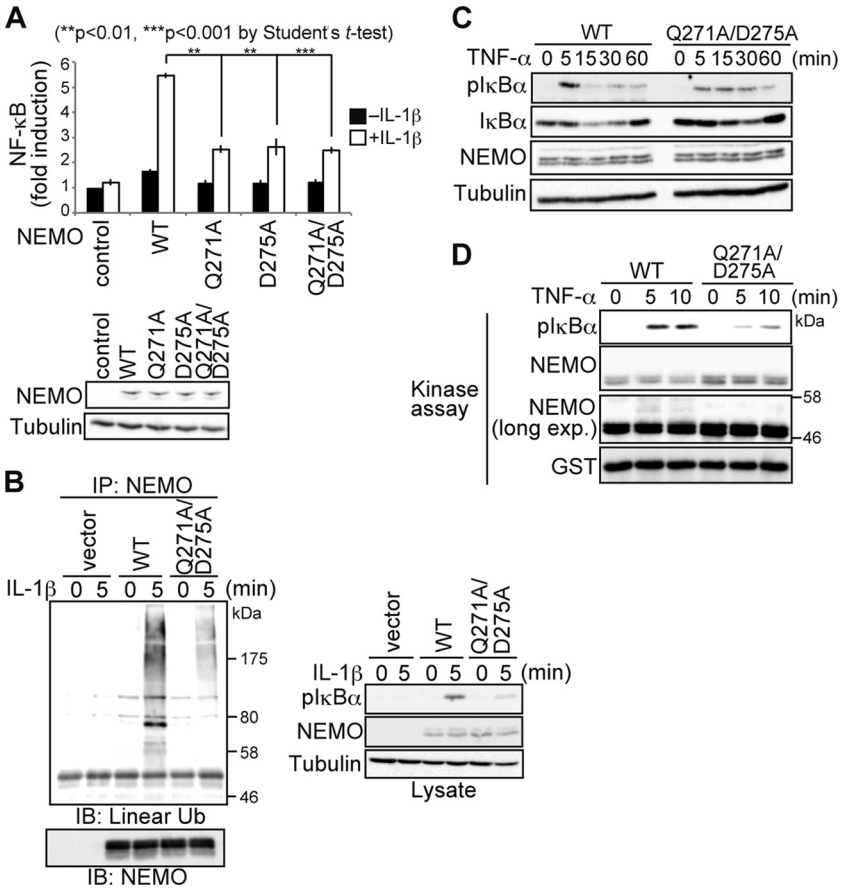

FIG 5 Conjugation of linear chains to NEMO plays crucial roles in IKK activation. (A) NEMO-defective N-1 cells were transiently transfected with 5× NF-κB luciferase reporter and WT or mutant NEMO. At 16 h after transfection, cells were treated with IL-1β (1 ng/ml) for 8 h, and luciferase activity was measured (means ± standard errors of the means; $n = 3$). The amounts of NEMO and tubulin were also assessed. (B) N-1 cells expressing WT or Q271A/D275A NEMO were treated with IL-1β (20 ng/ml) for the indicated periods, and anti-NEMO immunoprecipitates were immunoblotted. (C) NEMO-deficient MEFs stably expressing WT or Q271A/D275A NEMO were treated with TNF-α (10 ng/ml) for the indicated periods, and cell lysates were immunoblotted with the indicated antibodies. (D) Anti-NEMO immunoprecipitates from NEMO-deficient MEFs stably expressing WT or Q271A/D275A NEMO treated with TNF-α (10 ng/ml) for the indicated periods were incubated with GST-IκBα (amino acids 1 to 54) at 30°C for 2 h. The reaction mixtures were probed with the indicated antibodies.

conjugation of linear chains to NEMO and recognition of linear ubiquitin chains by NEMO are synergistically involved in signal-induced NF-κB activation.

IKK2, a crucial kinase within the IKK complex that phosphorylates IκBα, homodimerizes via its kinase domain (KD), leading to activation of IKK via *trans* autophosphorylation (30). We examined the involvement of KD homodimerization of IKK2 in the activation of IKK provoked by linearly ubiquitinated NEMO. Val229, His232, Tyr294, Gly295, and Pro296 of human IKK2 are involved in the KD-KD interaction of IKK2 (30). Therefore, we mutated Val229 and His232 to Ala (V229A/H232A); in another construct, Tyr294, Gly295, and Pro296 were mutated to Leu, Lys, and Gln, respectively, the corresponding amino acids in IKK1 (Y294L/G295K/P296Q) (30). IKK becomes constitutively active when Ser177 and Ser181 in the activation loop of IKK2 are mutated to phosphomimetic Glu (S177E/S181E) (30). V229A/Y232A and Y294L/G295K/P296Q IKK2 with the S177E/S181E mutations can effectively phosphorylate IκBα (30), suggesting that both of these IKK2 mutants can function as a kinase when specific Ser residues are phosphorylated. NEMO-Ub_2, a NEMO mutant with uncleavable linear diubiquitin at the C terminus, mimics linearly ubiquitinated NEMO, and the introduction of NEMO-Ub_2 alone to HEK293T cells induces IKK activation (15). With these observations in mind, we evaluated mutations of IKK2 that abolish the KD-KD interaction upon NEMO-Ub_2-mediated activation of IKK. Because IKK2 can be activated even when transiently introduced alone (30), we introduced smaller amounts of IKK2 plasmids into HEK293T cells than in previous studies. As expected, under these assay conditions, the IKK2 WT or mutants were not activated when IKK2 was introduced alone (Fig. 6B). When introduced together with NEMO, WT IKK2 was weakly phosphorylated in its activation loop; because IKK2 in NEMO-deficient cells is not effectively activated (31), this phosphorylation may have been due to an IKK2-NEMO interaction. We have observed that NEMO-Ub_2 induces phosphorylation of WT IKK2 much more efficiently than NEMO. However, NEMO-Ub_2 failed to induce phosphorylation of V229A/Y232A or Y294L/G295K/P296Q IKK2, indicating that the KD-KD interaction is necessary for the activation of IKK2 by NEMO-Ub_2. Because V229A/Y232A and Y294L/G295K/P296Q IKK2 could form complexes with NEMO and NEMO-Ub_2, as well as WT IKK2 (Fig. 6C), these observations indicate that recognition of the linear chain conjugated to NEMO,

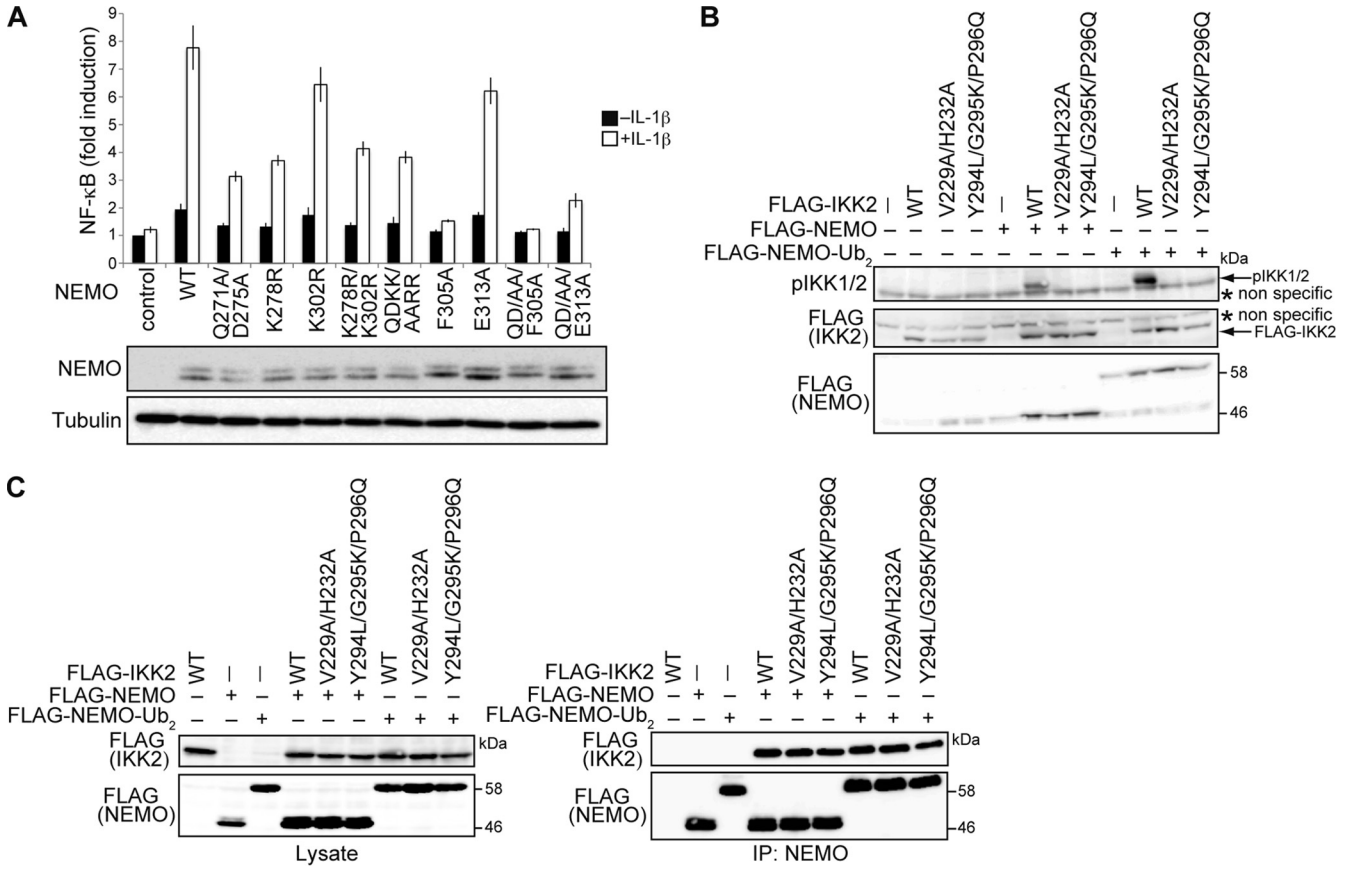

FIG 6 Mechanism underlying IKK activation mediated by LUBAC. (A) NEMO-defective N-1 cells were transiently transfected with 5× NF-κB luciferase reporter and WT or mutant NEMO. At 16 h after transfection, cells were treated with IL-1β (1 ng/ml) for 8 h, and luciferase activity was measured (means ± standard errors of the means; $n = 3$). The amounts of NEMO and tubulin were also assessed. (B) FLAG-IKK2 or its mutants, along with FLAG-NEMO or FLAG-NEMO-Ub_2, were transfected into HEK293T cells; cell lysates were immunoblotted with the indicated antibodies. (C) FLAG-IKK2 and its mutants, along with FLAG-NEMO or FLAG-NEMO-Ub_2, were transfected into HEK293T cells and cell lysates (left); anti-NEMO immunoprecipitates (right) were immunoblotted as indicated.

possibly by another NEMO molecule, plays crucial roles in IKK activation and subsequent NF-κB activation by inducing *trans* autophosphorylation of IKK2.

The NEMO- and ubiquitin-binding activities of HOIP NZF1 are both involved in NF-κB activation by LUBAC. Our crystallographic analyses revealed that HOIP NZF1 is involved in NEMO recognition and that Arg369 in the NZF1 domain of mouse HOIP (equivalent to Arg375 in human HOIP, used for the crystallographic analyses described above) contributes significantly to interaction with NEMO (Fig. 3G). However, NZF domains are classified as potential ubiquitin-binding modules (28, 32), and HOIP NZF1 has also been reported to bind ubiquitin (11). The highly conserved TF/Φ motif of NZF domains ("Φ" indicates a hydrophobic residue that is separated from TF [Thr-Phe] by 10 residues [33]) is crucial for the ubiquitin-binding activity (33). Because Thr354 and Phe355 of the TF/Φ motif in mouse HOIP NZF1 (equivalent to Thr360 and Phe361 in human HOIP) are highly conserved (Fig. 3J), it is reasonable to speculate that HOIP NZF1 might exhibit the ubiquitin-binding activity as well as NEMO-binding activity. To confirm the ability of NZF1 to bind ubiquitin, we generated R369A, T354A, F355A, and T354A/F355A mutations of mouse HOIP NZF1. GST pulldown assays revealed that the T354A, F355A, and T354A/F355A mutations, but not R369A, attenuated binding of HOIP NZF1 to not only Lys63-linked diubiquitin but also linear tetraubiquitin (Fig. 7A and B). To investigate the effect of the T354A, F355A, and T354A/F355A mutations on NEMO binding, we cotransfected WT or mutant HOIP into HEK293T cells along with HOIL-1L, SHARPIN, and NEMO. WT, T354A, F355A, and T354A/F355A HOIP efficiently coimmunoprecipitated with NEMO, whereas the ΔNZF1 and R369A HOIP mutants failed to interact with NEMO (Fig. 7C). From these results, we draw the following conclusions: NZF1 can bind to both ubiquitin and NEMO, Arg369 of HOIP NZF1 is involved in NEMO recognition but not ubiquitin binding, and T354 and F355 are involved in ubiquitin recognition but not NEMO binding. Furthermore, the *in vitro* binding assay using purified proteins revealed that NZF1 and Lys63-linked diubiquitin were both pulled down with MBP-NEMO, indicating that NZF1 bound simultaneously to Lys63-linked diubiquitin and NEMO (Fig. 7D).

To probe the roles of the ubiquitin- and NEMO-binding activities of NZF1 of HOIP in LUBAC-mediated NF-κB activation, we used luciferase assays to evaluate NF-κB activation mediated by exogenously introduced LUBAC. LUBAC-mediated NF-κB activation was suppressed in HEK293T cells transfected with R369A or ΔNZF1 HOIP. Introduction of T354A/F355A HOIP also suppressed LUBAC-mediated NF-κB activation, but the suppression

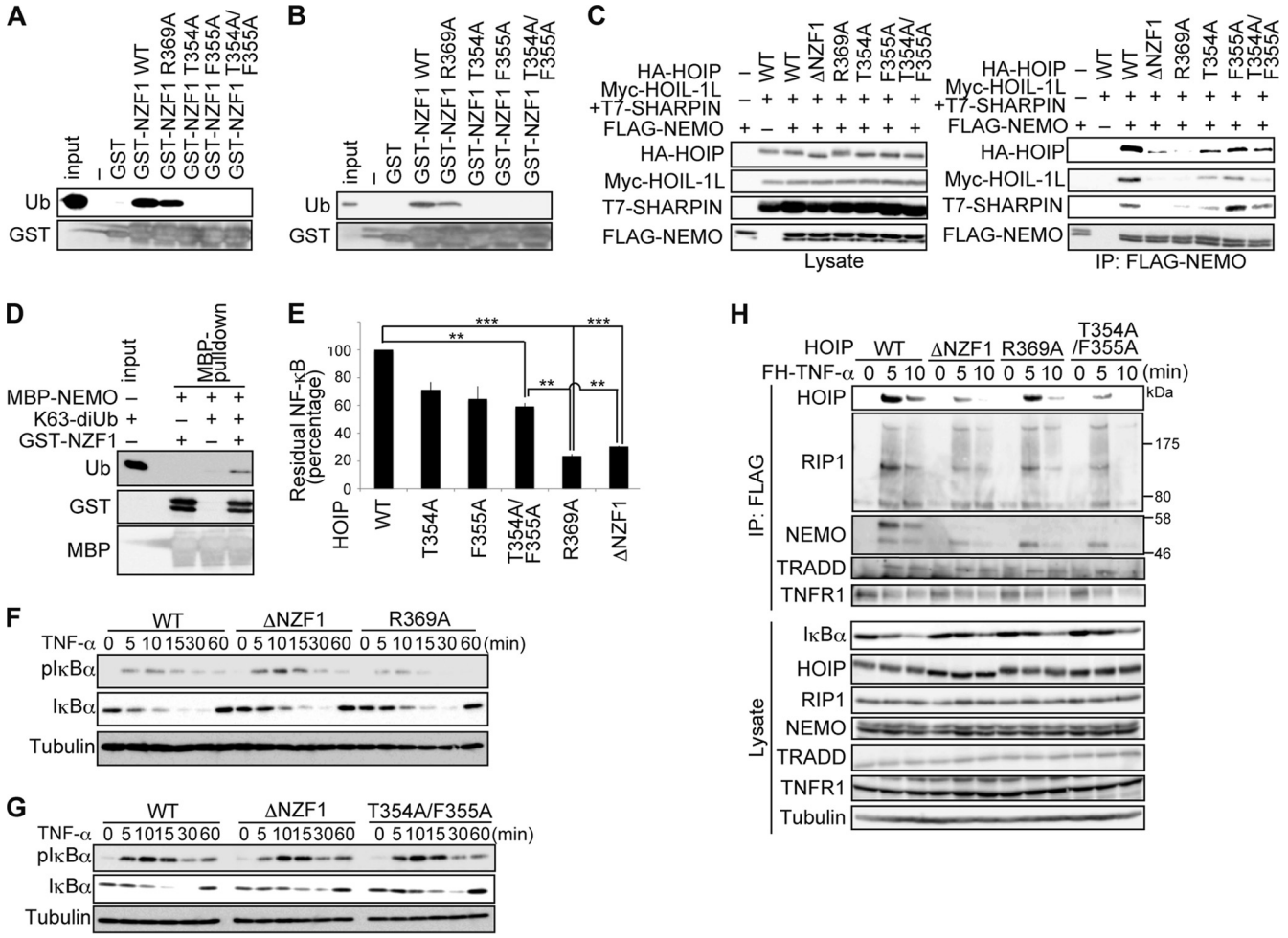

FIG 7 Simultaneous recognition of NEMO and ubiquitin by HOIP NZF1 is required for NF-κB activation. (A and B) WT or mutant HOIP NZF1 fused to GST was incubated with K63 diubiquitin (A) or linear tetraubiquitin (B) as indicated, followed by pulldown with glutathione beads. Bound proteins were probed as indicated. (C) HA-HOIP or its mutants were transfected into HEK293T cells along with Myc-HOIL-1L, T7-SHARPIN, and FLAG-NEMO, and cell lysates (left) and anti-FLAG immunoprecipitates (right) were immunoblotted as indicated. (D) Full-length NEMO fused with MBP was incubated with K63-diubiquitin and GST-NZF1, followed by pulldown with maltose resins. Bound proteins were probed as indicated. (E) Luciferase activities in HEK293T cells expressing WT or mutant HA-HOIP, along with Myc-HOIL-1L, T7-SHARPIN, and 5× NF-κB luciferase reporter, are shown relative to the activity in cells expressing WT LUBAC, defined as 100% (means ± standard errors of the means; $n = 3$). **, $P < 0.01$; ***, $P < 0.001$ (Student's t test). (F and G) HOIP Δlinear MEFs retrovirally expressing WT, ΔNZF1, or R369A (F) or T354A/F355A (G) HOIP were treated with TNF-α (3 ng/ml) for the indicated periods and probed with the indicated antibodies. (H) HOIP Δlinear MEFs retrovirally expressing WT, ΔNZF1, R369A, or T354A/F355A HOIP were treated with FLAG-His_6–TNF-α (FH-TNF-α) (3 μg/ml) for the indicated periods; cell lysates (bottom) and anti-FLAG immunoprecipitates (top) were immunoblotted as indicated.

was significantly weaker than that mediated by R369A HOIP (Fig. 7E). To further examine the roles of the ubiquitin- and NEMO-binding activities of HOIP NZF1 in TNF-α-mediated NF-κB activation, we introduced WT or HOIP mutants into HOIP Δlinear MEFs; the HOIP mutants were expressed at levels identical to or a little higher than that of WT HOIP (data not shown). In cells expressing R369A or T354A/F355A HOIP, IκBα degradation was slower than in WT HOIP-expressing cells; the extent of the delay with these two mutants was similar to that with ΔNZF1 HOIP (Fig. 7F and G). The ubiquitin-binding activity of HOIP has been implicated in the recruitment of LUBAC to the activated TNF-R1 signaling complex (TNF-RSC) (34). ΔNZF and T354A/F355A mutations of HOIP attenuated TNF-α-induced recruitment of HOIP to TNF-RSC, but the R369A mutation did not overtly suppress HOIP recruitment to the activated receptor complex (Fig. 7H). Importantly, WT HOIP and the R369A mutant were recruited to TNF-RSC at similar levels, but ubiquitination of NEMO was significantly abrogated by the R369A mutation.

These results strongly indicated that NZF1 of HOIP can simultaneously bind both NEMO and ubiquitin and that both interactions are involved in TNF-α-mediated NF-κB activation. Loss of NEMO binding impairs linear polyubiquitination of NEMO, whereas loss of ubiquitin binding impairs recruitment of LUBAC to TNF-RSC. However, loss of NEMO binding by HOIP NZF1 appears to exert a more profound effect on LUBAC-mediated NF-κB activation than loss of ubiquitin binding. Although the interaction between HOIP NZF1 and NEMO was abolished almost completely by the mutations described above, neither TNF-α- nor LUBAC-mediated NF-κB activation was completely suppressed in cells expressing these mutants.

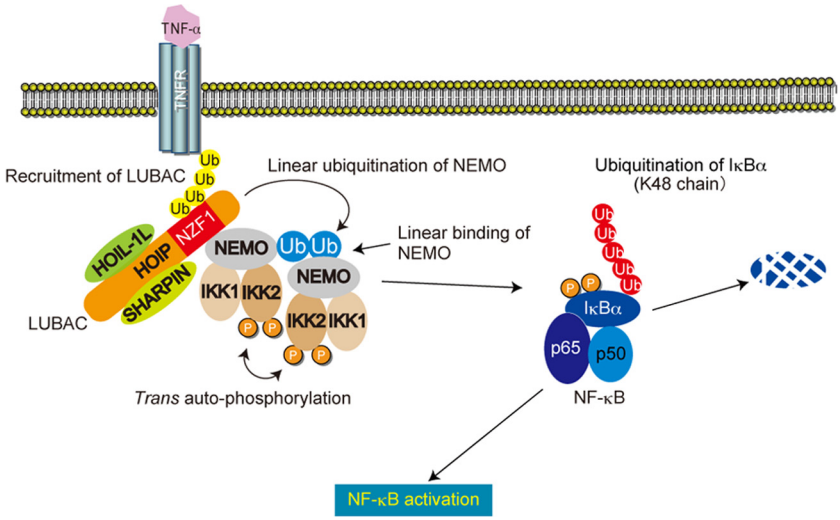

FIG 8 Schematic representation of LUBAC-mediated IKK and NF-κB activation. Upon ligand stimulation, LUBAC is recruited to the receptor via the ubiquitin-binding ability of HOIP NZF1. Then, HOIP NZF1 also recognizes NEMO, and this recognition is involved in linear polyubiquitination of NEMO. Linear chains conjugated to NEMO are recognized by NEMO in *trans* on another IKK complex, thereby inducing multimerization of the IKK complex and *trans* autophosphorylation of IKK2.

We propose mechanisms that might underlie this residual NF-κB activation in Discussion.

DISCUSSION

In this study, we showed that recognition of linear ubiquitin chains by NEMO and conjugation of those chains to NEMO are synergistically involved in IKK activation. The IKK complex is activated by phosphorylation of the IKK2 subunit (35). In general, phosphorylation of kinases is mediated either by *trans* autophosphorylation or by upstream kinases (36). The crystal structure of *Xenopus* IKK2, determined recently, reveals that IKK2 contains a dimerization domain (31); dimerization-defective IKK2 mutants fail to be activated. Furthermore, analysis of the crystal structure of human IKK2 revealed that homotypic interaction of the IKK2 KD is crucial for IKK2 activation (30). We also showed that IKK2 mutants that are defective in KD-KD interaction could not be activated by NEMO-Ub_2, which mimics linearly ubiquitinated NEMO. These results strongly indicate that IKK2 activation mediated by linear chains requires *trans* autophosphorylation; thus, it seems plausible that linear chains conjugated to NEMO by LUBAC are recognized by NEMO in *trans* on another IKK complex, thereby inducing multimerization of IKK complexes. Upon multimerization, IKK2 could dimerize and *trans* autophosphorylate (Fig. 8). It is possible that binding of ubiquitin to the UBAN domain induces conformational changes in NEMO, thereby changing the positions of IKK1 and IKK2, leading to phosphorylation of IKK2. However, considering the results of structural analyses of IKK2, together with our observations, the former scenario seems more likely (37).

We have probed the interactions between HOIP and NEMO by solving a cocrystal structure of NZF1 of human HOIP and CoZi of mouse NEMO, while our mutational studies have been performed using mouse HOIP. However, the surface residues from HOIP that interact with NEMO are fully conserved in human and mouse species (Fig. 3J). Our mutational analyses based on the structure of the cocrystal show that direct recognition of NEMO by HOIP plays a major role in NF-κB activation following conjugation of linear chains to NEMO. Although the RING-IBR-RING region of HOIP is the catalytic center for linear polyubiquitination by LUBAC (7), recent results obtained using an *in vitro* ubiquitin assay have suggested that the RING2 domain of HOIL-1L plays a role in linear polyubiquitination of NEMO (38). However, given that the HOIP-SHARPIN complex effectively linearly polyubiquitinates NEMO *in vitro* and activates NF-κB in cells (12), any involvement of the RING2 domain of HOIL-1L in linear polyubiquitination of NEMO and NF-κB activation seems likely to be marginal. Thus, HOIP plays central roles in LUBAC-mediated NF-κB activation via direct recognition of linear polyubiquitin and conjugation of this molecule to NEMO. However, neither NF-κB activation nor linear polyubiquitination of NEMO was completely abolished in Q271A/D275A NEMO, which evades recognition by LUBAC. We suspect that the residual activation might be caused by the presence of one or more additional NEMO recognition sites. Consistent with this idea, the NEMO-LUBAC interaction cannot be completely abolished by mutations in HOIP NZF1, although HOIP NZF1 does appear to be the primary NEMO recognition site. In support of this possibility, in our previous study (8), we observed that HOIP lacking NZF1 could bind NEMO in the presence of high levels of HOIL-1L. Alternatively, in light of observations that the linear polyubiquitination activity of LUBAC is dispensable for NF-κB activation via B-cell antigen receptor (39), residual NF-κB activation might be mediated by other IKK activation pathways. The kinase TAK1 has been suggested to activate IKK2 (40); specifically, TAK1-mediated IKK activation has been proposed to involve the Lys63 chain-binding activity of TAB2 and TAB3, which form a complex with TAK1 (41). Recently, Lys63 and linear hybrid chains have been implicated in IKK activation (42). It is hypothesized that both the TAK1 and IKK complexes bind simultaneously to one hybrid chain composed of Lys63 and linear linkages, generated upon IL-1β stimulation, thereby inducing phosphorylation of IKK2 (42). In addition to the UBAN motif that preferentially binds linear

chains, NEMO possesses another ubiquitin-binding domain, the ZF domain, in its C terminus. NEMO can bind longer Lys63-linked chains by utilizing both the UBAN and ZF domains, potentially inducing IKK activation by multimerizing the IKK complex. Because the NEMO-LUBAC interaction appears dispensable for the generation of the Lys63 and Lys63/linear hybrid chains, the residual NF-κB activation in Q271A/D275A NEMO-expressing cells might be attributed to these ubiquitin chains, as distinct from linear chains. However, considering our results described here, together with the previous observation that Lys63-linked chains are dispensable for TNF-α-mediated NF-κB activation (43), it seems likely that linear chain-mediated *trans* autophosphorylation of IKK2 plays a major role in NF-κB activation, at least in the case of activation mediated by the TNF receptor family. In further support of this notion, we observed previously that CD40-mediated NF-κB activation is almost completely abolished in B cells from mice lacking the linear polyubiquitination activity of LUBAC (39). Further dissection of the mechanism underlying IKK activation via LUBAC-mediated linear polyubiquitination will be needed to clarify the involvement of linear chain-mediated dimerization of IKK2 in NF-κB activation induced by various stimuli, including IL-1β.

We also showed here that HOIP NZF1 simultaneously binds NEMO and ubiquitin (Fig. 7D). The TF/Φ motifs of the HOIP NZF domains, which are crucial for ubiquitin binding by NZFs, are highly conserved. Consistent with this, the T354A, F355A, and T354A/F355A mutants of HOIP NZF1 failed to bind ubiquitin. In contrast, R369A NZF1 could bind ubiquitin as efficiently as WT NZF1 (Fig. 7A and B). Recruitment of LUBAC to TNF-RSC upon TNF-α stimulation is a prerequisite for TNF-α-mediated NF-κB activation, and the ubiquitin-binding activity of LUBAC is required for this recruitment (34). We observed in this study that the T354A/F355A double mutation, but not the R369A mutation, of HOIP attenuated TNF-α-induced recruitment of HOIP to TNF-RSC (Fig. 7H). Furthermore, we observed that both R369A and T354A/F355A HOIP attenuated TNF-α-induced NF-κB activation at a level comparable to that of ΔNZF1 HOIP when expressed in HOIP Δlinear MEFs (Fig. 7F and G). However, the luciferase assays revealed that R369A, but not T354A, F355A, or T354A/F355A, HOIP significantly suppressed NF-κB activation induced by the introduction of LUBAC components (Fig. 7E). Recruitment of LUBAC to TNF-RSC is a prerequisite for TNF-α-mediated NF-κB activation but is apparently not required for NF-κB activation provoked by the exogenous introduction of LUBAC components; this may explain why the R369A mutation of HOIP suppressed LUBAC-mediated NF-κB activation more severely than the T354A/F355A mutation.

In summary, we dissected the roles of linear polyubiquitination in NF-κB activation and showed that recognition of linear polyubiquitin conjugated to NEMO, possibly by NEMO in another IKK complex, induces *trans* autophosphorylation of IKK2 and subsequent activation of NF-κB. The NZF1 domain of HOIP is involved in the linear polyubiquitination of NEMO by recognizing NEMO, leading to the homodimerization of IKK2. In addition to NEMO recognition, HOIP NZF1 plays another role in signal-induced NF-κB activation: the recruitment of LUBAC to the activated receptor complexes via its ubiquitin-binding activity (Fig. 8). Amino acid residues crucial for ubiquitin binding are conserved in HOIP NZF1 (Fig. 3I), whereas other residues are not conserved in other human NZFs. In contrast, the NEMO-binding surface on HOIP NZF1 is highly conserved in NZF1s of vertebrate HOIP proteins (Fig. 3J). Because HOIP NZF1 can bind to both ubiquitin and NEMO simultaneously (Fig. 7D), we conclude that HOIP NZF1 plays a critical role in signal-induced activation by recruiting LUBAC to the site of function and ubiquitinating the substrate to activate NF-κB on site.

ACKNOWLEDGMENTS

We thank T. Kitamura, R. Baker, and H. Kamata for providing pMX-IP, USP2cc, and NEMO-deficient MEFs, respectively.

This work was partly supported by the Targeted Proteins Research Program (TPRP) and grants from the Ministry of Education, Culture, Sports, Science, and Technology of Japan to K.I. and S.W. S.R. was a recipient of the JSPS Invitation Fellowship for Research in Japan (long-term).

REFERENCES

1. **Vallabhapurapu S, Karin M.** 2009. Regulation and function of NF-κB transcription factors in the immune system. Annu. Rev. Immunol. **27:** 693–733. http://dx.doi.org/10.1146/annurev.immunol.021908.132641.
2. **Karin M.** 2006. Nuclear factor-κB in cancer development and progression. Nature **441:**431–436. http://dx.doi.org/10.1038/nature04870.
3. **Li Q, Verma IM.** 2002. NF-κB regulation in the immune system. Nat. Rev. Immunol. **2:**725–734. http://dx.doi.org/10.1038/nri910.
4. **Baltimore D.** 2011. NF-κB is 25. Nat. Immunol. **12:**683–685. http://dx.doi.org/10.1038/ni.2072.
5. **Hayden MS, Ghosh S.** 2008. Shared principles in NF-κB signaling. Cell **132:**344–362. http://dx.doi.org/10.1016/j.cell.2008.01.020.
6. **Skaug B, Jiang X, Chen ZJ.** 2009. The role of ubiquitin in NF-κB regulatory pathways. Annu. Rev. Biochem. **78:**769–796. http://dx.doi.org/10.1146/annurev.biochem.78.070907.102750.
7. **Kirisako T, Kamei K, Murata S, Kato M, Fukumoto H, Kanie M, Sano S, Tokunaga F, Tanaka K, Iwai K.** 2006. A ubiquitin ligase complex assembles linear polyubiquitin chains. EMBO J. **25:**4877–4887. http://dx.doi.org/10.1038/sj.emboj.7601360.
8. **Tokunaga F, Sakata S, Saeki Y, Satomi Y, Kirisako T, Kamei K, Nakagawa T, Kato M, Murata S, Yamaoka S, Yamamoto M, Akira S, Takao T, Tanaka K, Iwai K.** 2009. Involvement of linear polyubiquitylation of NEMO in NF-κB activation. Nat. Cell Biol. **11:**123–132. http://dx.doi.org/10.1038/ncb1821.
9. **Boisson B, Laplantine E, Prando C, Giliani S, Israelsson E, Xu Z, Abhyankar A, Israel L, Trevejo-Nunez G, Bogunovic D, Cepika AM, MacDuff D, Chrabieh M, Hubeau M, Bajolle F, Debre M, Mazzolari E, Vairo D, Agou F, Virgin HW, Bossuyt X, Rambaud C, Facchetti F, Bonnet D, Quartier P, Fournet JC, Pascual V, Chaussabel D, Notarangelo LD, Puel A, Israel A, Casanova JL, Picard C.** 2012. Immunodeficiency, autoinflammation and amylopectinosis in humans with inherited HOIL-1 and LUBAC deficiency. Nat. Immunol. **13:**1178–1186. http://dx.doi.org/10.1038/ni.2457.
10. **Gerlach B, Cordier SM, Schmukle AC, Emmerich CH, Rieser E, Haas TL, Webb AI, Rickard JA, Anderton H, Wong WW, Nachbur U, Gangoda L, Warnken U, Purcell AW, Silke J, Walczak H.** 2011. Linear ubiquitination prevents inflammation and regulates immune signalling. Nature **471:**591–596. http://dx.doi.org/10.1038/nature09816.
11. **Ikeda F, Deribe YL, Skanland SS, Stieglitz B, Grabbe C, Franz-Wachtel M, van Wijk SJ, Goswami P, Nagy V, Terzic J, Tokunaga F, Androulidaki A, Nakagawa T, Pasparakis M, Iwai K, Sundberg JP, Schaefer L, Rittinger K, Macek B, Dikic I.** 2011. SHARPIN forms a linear ubiquitin ligase complex regulating NF-κB activity and apoptosis. Nature **471:**637–641. http://dx.doi.org/10.1038/nature09814.
12. **Tokunaga F, Nakagawa T, Nakahara M, Saeki Y, Taniguchi M, Sakata S, Tanaka K, Nakano H, Iwai K.** 2011. SHARPIN is a component of the NF-κB-activating linear ubiquitin chain assembly complex. Nature **471:**633–636. http://dx.doi.org/10.1038/nature09815.
13. **Saito N, Courtois G, Chiba A, Yamamoto N, Nitta T, Hironaka N, Rowe M, Yamaoka S.** 2003. Two carboxyl-terminal activation regions of Epstein-Barr virus latent membrane protein 1 activate NF-κB through distinct signaling pathways in fibroblast cell lines. J. Biol. Chem. **278:**46565–46575. http://dx.doi.org/10.1074/jbc.M302549200.
14. **Catanzariti AM, Soboleva TA, Jans DA, Board PG, Baker RT.** 2004. An

efficient system for high-level expression and easy purification of authentic recombinant proteins. Protein Sci. **13:**1331–1339. http://dx.doi.org/10.1110/ps.04618904.

15. **Kensche T, Tokunaga F, Ikeda F, Goto E, Iwai K, Dikic I.** 2012. Analysis of nuclear factor-κB (NF-κB) essential modulator (NEMO) binding to linear and lysine-linked ubiquitin chains and its role in the activation of NF-κB. J. Biol. Chem. **287:**23626–23634. http://dx.doi.org/10.1074/jbc.M112.347195.
16. **Otwinowski Z, Minor W.** 1997. Processing of X-ray diffraction data collected in oscillation mode. Methods Enzymol. **276:**307–326. http://dx.doi.org/10.1016/S0076-6879(97)76066-X.
17. **Leslie AW, Powell H.** 2007. Processing diffraction data with mosflm. NATO Sci. Ser. **245:**41–51. http://dx.doi.org/10.1007/978-1-4020-6316-9_4.
18. **Vagin A, Teplyakov A.** 1997. MOLREP: an automated program for molecular replacement. J. Appl. Crystallogr. **30:**1022–1025. http://dx.doi.org/10.1107/S0021889897006766.
19. **Lo YC, Lin SC, Rospigliosi CC, Conze DB, Wu CJ, Ashwell JD, Eliezer D, Wu H.** 2009. Structural basis for recognition of diubiquitins by NEMO. Mol. Cell **33:**602–615. http://dx.doi.org/10.1016/j.molcel.2009.01.012.
20. **Sato Y, Yoshikawa A, Yamashita M, Yamagata A, Fukai S.** 2009. Structural basis for specific recognition of Lys 63-linked polyubiquitin chains by NZF domains of TAB2 and TAB3. EMBO J. **28:**3903–3909. http://dx.doi.org/10.1038/emboj.2009.345.
21. **Emsley P, Cowtan K.** 2004. Coot: model-building tools for molecular graphics. Acta Crystallogr. D Biol. Crystallogr. **60:**2126–2132. http://dx.doi.org/10.1107/S0907444904019158.
22. **Murshudov GN, Skubak P, Lebedev AA, Pannu NS, Steiner RA, Nicholls RA, Winn MD, Long F, Vagin AA.** 2011. REFMAC5 for the refinement of macromolecular crystal structures. Acta Crystallogr. D Biol. Crystallogr. **67:**355–367. http://dx.doi.org/10.1107/S0907444911001314.
23. **Murshudov GN, Vagin AA, Dodson EJ.** 1997. Refinement of macromolecular structures by the maximum-likelihood method. Acta Crystallogr. D Biol. Crystallogr. **53:**240–255. http://dx.doi.org/10.1107/S0907444996012255.
24. **Rahighi S, Ikeda F, Kawasaki M, Akutsu M, Suzuki N, Kato R, Kensche T, Uejima T, Bloor S, Komander D, Randow F, Wakatsuki S, Dikic I.** 2009. Specific recognition of linear ubiquitin chains by NEMO is important for NF-κB activation. Cell **136:**1098–1109. http://dx.doi.org/10.1016/j.cell.2009.03.007.
25. **Smit JJ, Monteferrario D, Noordermeer SM, van Dijk WJ, van der Reijden BA, Sixma TK.** 2012. The E3 ligase HOIP specifies linear ubiquitin chain assembly through its RING-IBR-RING domain and the unique LDD extension. EMBO J. **31:**3833–3844. http://dx.doi.org/10.1038/emboj.2012.217.
26. **Jackson PK, Eldridge AG, Freed E, Furstenthal L, Hsu JY, Kaiser BK, Reimann JD.** 2000. The lore of the RINGs: substrate recognition and catalysis by ubiquitin ligases. Trends Cell Biol. **10:**429–439. http://dx.doi.org/10.1016/S0962-8924(00)01834-1.
27. **Ivins FJ, Montgomery MG, Smith SJ, Morris-Davies AC, Taylor IA, Rittinger K.** 2009. NEMO oligomerization and its ubiquitin-binding properties. Biochem. J. **421:**243–251. http://dx.doi.org/10.1042/BJ20090427.
28. **Wang B, Alam SL, Meyer HH, Payne M, Stemmler TL, Davis DR, Sundquist WI.** 2003. Structure and ubiquitin interactions of the conserved zinc finger domain of Npl4. J. Biol. Chem. **278:**20225–20234. http://dx.doi.org/10.1074/jbc.M300459200.
29. **Laplantine E, Fontan E, Chiaravalli J, Lopez T, Lakisic G, Veron M, Agou F, Israel A.** 2009. NEMO specifically recognizes K63-linked polyubiquitin chains through a new bipartite ubiquitin-binding domain. EMBO J. **28:**2885–2895. http://dx.doi.org/10.1038/emboj.2009.241.
30. **Polley S, Huang DB, Hauenstein AV, Fusco AJ, Zhong X, Vu D, Schrofelbauer B, Kim Y, Hoffmann A, Verma IM, Ghosh G, Huxford T.** 2013. A structural basis for IκB kinase 2 activation via oligomerization-dependent trans auto-phosphorylation. PLoS Biol. **11:**e1001581. http://dx.doi.org/10.1371/journal.pbio.1001581.
31. **Xu G, Lo YC, Li Q, Napolitano G, Wu X, Jiang X, Dreano M, Karin M, Wu H.** 2011. Crystal structure of inhibitor of κB kinase β. Nature **472:**325–330. http://dx.doi.org/10.1038/nature09853.
32. **Meyer HH, Wang Y, Warren G.** 2002. Direct binding of ubiquitin conjugates by the mammalian p97 adaptor complexes, p47 and Ufd1-Npl4. EMBO J. **21:**5645–5652. http://dx.doi.org/10.1093/emboj/cdf579.
33. **Alam SL, Sun J, Payne M, Welch BD, Blake BK, Davis DR, Meyer HH, Emr SD, Sundquist WI.** 2004. Ubiquitin interactions of NZF zinc fingers. EMBO J. **23:**1411–1421. http://dx.doi.org/10.1038/sj.emboj.7600114.
34. **Haas TL, Emmerich CH, Gerlach B, Schmukle AC, Cordier SM, Rieser E, Feltham R, Vince J, Warnken U, Wenger T, Koschny R, Komander D, Silke J, Walczak H.** 2009. Recruitment of the linear ubiquitin chain assembly complex stabilizes the TNF-R1 signaling complex and is required for TNF-mediated gene induction. Mol. Cell **36:**831–844. http://dx.doi.org/10.1016/j.molcel.2009.10.013.
35. **Israel A.** 2010. The IKK complex, a central regulator of NF-κB activation. Cold Spring Harbor Perspect. Biol. **2:**a000158. http://dx.doi.org/10.1101/cshperspect.a000158.
36. **Hunter T, Lindberg RA, Middlemas DS, Tracy S, van der Geer P.** 1992. Receptor protein tyrosine kinases and phosphatases. Cold Spring Harbor Symp. Quant. Biol. **57:**25–41. http://dx.doi.org/10.1101/SQB.1992.057.01.005.
37. **Iwai K.** 2012. Diverse ubiquitin signaling in NF-κB activation. Trends Cell Biol. **22:**355–364. http://dx.doi.org/10.1016/j.tcb.2012.04.001.
38. **Smit JJ, van Dijk WJ, El Atmioui D, Merkx R, Ovaa H, Sixma TK.** 2013. Target specificity of the E3 ligase LUBAC for ubiquitin and NEMO relies on different minimal requirements. J. Biol. Chem. **288:**31728–31737. http://dx.doi.org/10.1074/jbc.M113.495846.
39. **Sasaki Y, Sano S, Nakahara M, Murata S, Kometani K, Aiba Y, Sakamoto S, Watanabe Y, Tanaka K, Kurosaki T, Iwai K.** 2013. Defective immune responses in mice lacking LUBAC-mediated linear ubiquitination in B cells. EMBO J. **32:**2463–2476. http://dx.doi.org/10.1038/emboj.2013.184.
40. **Wang C, Deng L, Hong M, Akkaraju GR, Inoue J, Chen ZJ.** 2001. TAK1 is a ubiquitin-dependent kinase of MKK and IKK. Nature **412:**346–351. http://dx.doi.org/10.1038/35085597.
41. **Kanayama A, Seth RB, Sun L, Ea CK, Hong M, Shaito A, Chiu YH, Deng L, Chen ZJ.** 2004. TAB2 and TAB3 activate the NF-κB pathway through binding to polyubiquitin chains. Mol. Cell **15:**535–548. http://dx.doi.org/10.1016/j.molcel.2004.08.008.
42. **Emmerich CH, Ordureau A, Strickson S, Arthur JS, Pedrioli PG, Komander D, Cohen P.** 2013. Activation of the canonical IKK complex by K63/M1-linked hybrid ubiquitin chains. Proc. Natl. Acad. Sci. U. S. A. **110:**15247–15252. http://dx.doi.org/10.1073/pnas.1314715110.
43. **Xu M, Skaug B, Zeng W, Chen ZJ.** 2009. A ubiquitin replacement strategy in human cells reveals distinct mechanisms of IKK activation by TNFα and IL-1β. Mol. Cell **36:**302–314. http://dx.doi.org/10.1016/j.molcel.2009.10.002.